Geosciences

AIMS Geosciences, 11(2): 274–297.
DOI: 10.3934/geosci.2025012
Received: 03 November 2024
Revised: 21 February 2025
Accepted: 14 March 2025
Published: 14 April 2025

https://www.aimspress.com/journal/geosciences

Research article

Pre-eruption landslide as a possible cause of early tsunami waves from Tongo volcano on January 15, 2022

Raissa Mazova[1,*], Kirill Polyakov[1], Dmitry Smirnov[1], Ivan Smirnov[1], Andrey Kurkin[1,2] and Jorge Van Den Bosch F[3]

[1] Nizhny Novgorod State Technical University n.a. R.E. Alekseev, Nizhny Novgorod, Russia
[2] V.I. Il'ichev Pacific Oceanological Institute Far Eastern Branch Russian Academy of Sciences, Vladivostok, Russia
[3] Engineering Center Mitigation Natural Catastrophes Faculty of Engineering, University of Antofagasta, Antofagasta, Chile

* **Correspondence:** Email: raissamazova@yandex.ru.

Abstract: In this paper, a mechanism is proposed for the occurrence of "early" tsunami waves on various coasts of the Pacific Ocean, which arrived after the eruption of the Tonga volcano 4–5 hours earlier than the actual time of the tsunami wave arrival at a given sea level. The paper shows that Kthere is another alternative hypothesis about the generation of an early wave train by a pre-eruption landslide source, which is localized on the slope of the Tonga volcano, in addition to the hypothesis available in the literature explaining this phenomenon as the generation of tsunami waves by Lamb waves or caldera collapse. At the same time, during the period of preparing for the eruption, the trigger for the pre-eruption landslide process could have been both minor seismic foreshocks, which were numerous before the eruption, and the process of preparing for the volcanic eruption itself. Wave characteristics of the tsunami generated by the pre-eruption landslide process on the volcanic slope are obtained. A possible implementation of the pre-eruption landslide mechanism for generating "early" tsunami waves is presented by considering various scenarios of pre-eruption landslide source formation and taking the tsunami characteristics at specific sites into account.

Keywords: acoustic and long gravitational sea wave (tsunami); landslide process; numerical simulation; tsunami wave characteristics; volcanic eruption

1. Introduction

It is well known that the main cause of tsunami waves is underwater earthquakes. Much less common tsunamis are caused by landslides, meteorological causes, and volcanic eruptions [1]. Moreover, tsunamis of volcanic origin (i.e., volcanic tsunamis) can be generated by various mechanisms, including volcano-tectonic earthquakes, submarine landslides, atmospheric acoustic waves, and caldera collapse [2]. In this paper, one of the largest volcanic tsunamis in history, which was caused by the eruption of Hunga Tonga volcano in January 2022, is studied. On January 15, 2022, at 4:15 (UT), a major eruption of Hunga Tonga-Hunga Ha'apai volcano occurred. Hunga Tonga-Hunga Ha'apai is one of several active submarine volcanoes in the Kingdom of Tonga, an island archipelago in the southwestern Pacific Ocean (Figure 1) [3]. The volcano is located at a distance of more than 3200 km northeast of Australia, with the coordinates 20°32′36″ S and 175°23′33″ W [4]. The eruption of the Hunga – Tonga volcano was accompanied by a colossal explosion. The explosion was reportedly heard as far away as Alaska [5]. Hunga -Tonga is an active volcano formed by the westward subduction of the Pacific tectonic plate under the Australian Plate along the Tonga-Kermadec Trench, which is an oceanic trench in the southwest Pacific Ocean that extends between Samoa and New Zealand [2–4].

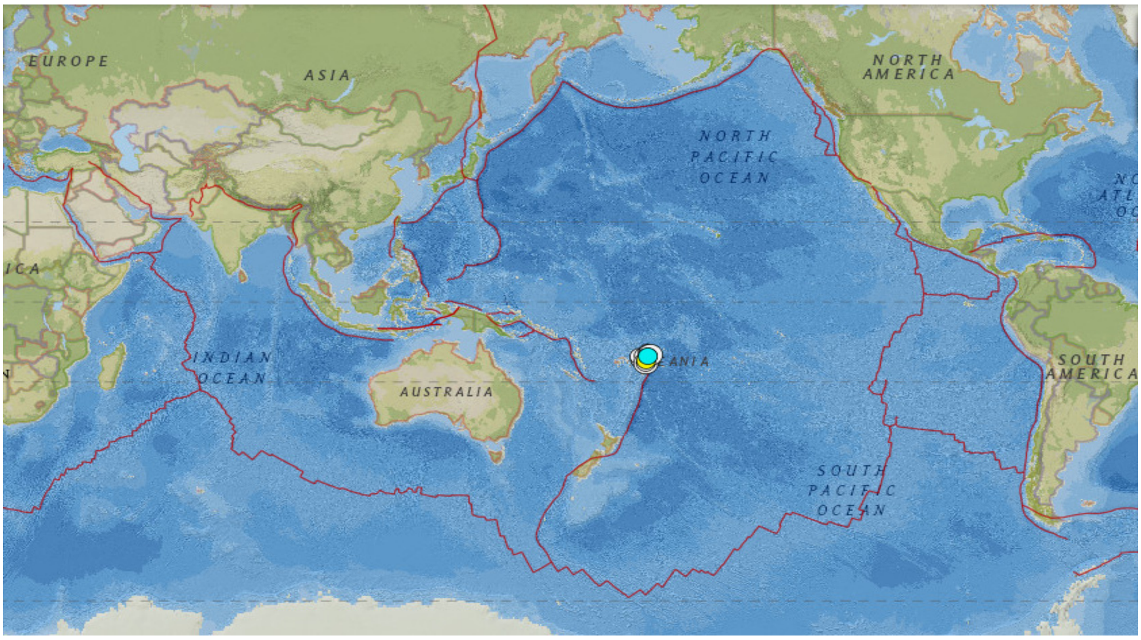

Figure 1. Location of the Tonga volcano on a geographical map. The red lines are tectonic plate boundaries [3].

The underwater eruption of Hunga Tonga is the largest since the 1883 eruption of Krakatoa, which was the most destructive volcanic tsunami in recorded history. On August 27, 1883, Krakatoa, a volcano in the Sunda Strait between Java and Sumatra, erupted four times within 5 hours, which generated a series of tsunami waves up to 40 meters high that destroyed hundreds of towns and villages. At least 36,000 people died [5–7]. The Hunga Tonga eruption generated numerous geophysical processes; however, the greatest interest to this study is the formation of acoustic-gravity waves and tsunami waves. The explosive nature of the eruption, which was accompanied by powerful movements of air masses, caused noticeable fluctuations in the atmospheric pressure over significant distances as a result of the propagation of Lamb acoustic waves. The explosion caused three direct and three reverse Lamb waves that circled the planet [4]. Another feature of this eruption is the tsunami that followed, the waves of which were recorded all over the world. It is noted that the first wave was the largest. According to eyewitnesses in the capital of the Kingdom of Tonga, a series of explosions were heard first, and the first tsunami was recorded about 15 minutes later. In total, three large waves (about 15 m) hit the coast of the Kingdom of Tonga [8]. It is noteworthy that even higher values were observed in the distant zone. Additionally, sea level fluctuations were recorded throughout the Pacific Ocean, as well as in the Atlantic and Indian Oceans [7]

Table 1. Data on the tsunami wave heights caused by eruption of the Tonga volcano [7].

Observation point	Wave height (m)	Observation point	Wave height (m)
Nuku'alofa (Kingdom of Tonga)	1.5 – 2	Kagoshima (Japan)	1.2
Hawaii (USA)	0.82	Tosashimizu (Japan)	0.9
Port San Luis (USA, CA)	1.3	Chichijima (Japan)	0.9
Arena Cove (USA, CA)	1.1	Tohoku(Japan)	0.7
South Coast of Oregon (USA)	more 0.3	Iwate(Japan)	1.1
New Zealand	more 1	Vodopadnaya Station (Russia, Kuril Islands)	1.4
Samoa (USA)	0.6	Guerrero, Colima, Baja California (Mexico)	0.61
Vanuatu	1–2.5	Manzanillo (Mexico)	2.05
Norfolk Island (Australia)	1.27	Zihuatanejo (Mexico)	1.19
Lord Howe Island (Australia)	1.10	Arica (Chile)	1.18
Gold Coast(Australia)	0.82	Coquimbo (Chile)	1.43
State of New South Wales (Australia)	0.5		

2. Analysis of data on acoustic and sea waves caused by the eruption of the Tonga volcano

The Hunga Tonga-Hunga Ha'apai tsunami is notable for its far-field occurrence, and showed higher propagation speeds, unexpected wave heights, and an unprecedented duration compared to seismically generated tsunamis [8,9]. In fact, the tsunami recorded worldwide arrived much earlier than would be expected from a tsunami generated by the Tonga eruption. A comparison of the propagation times between the possible tsunami generated at the time of the eruption and the observed tsunami waves which arrived at points on different coasts shows that the latter arrived 2.5 to 5 hours earlier, thereby crossing the Pacific, Atlantic, and Indian Oceans in less than 20 hours. This difference in propagation speed is primarily noticeable in the far-field. For example, the tsunami reached the coasts of Japan and Chile earlier than the waves that arrived after the volcanic eruption, that is, the propagation times of the tsunami waves to the coasts of Japan and Chile were less than 7 and 10 hours, respectively, which were much shorter than the propagation time of the tsunami from the explosion (i.e., 10.5–12.5 hours for Japan and 12–17 hours for Chile). In the Atlantic and Indian Oceans, the first tsunami waves arrived even earlier. They reached the Caribbean Sea in 10–11 hours, whereas the long waves generated by the explosion would have taken more than 26 hours to reach the Caribbean Sea from their source, around the South American continent. The same applies to the eastern coasts of the Atlantic and Mediterranean Seas, where ocean disturbances were observed after 16.5 hours in Portugal and 17.5 hours in Italy, while the arrival of the first normal waves was expected after 27 and 32 hours, respectively [10–12]. Analyzing these data, it can be suggested that the tsunami waves that formed could have been generated by several different mechanisms: presumably by the collapse of the caldera, by Lamb acoustic waves generated by the volcanic eruption [13], or by submarine landslides on the slope of the volcano that formed before the eruption during the preparation of the eruption. For example, according to Mauricio Fuentes [14], the observation of significant amplitudes at stations located at transoceanic distances suggests that "the formation of this tsunami is the sum of different types of sources and not just the eruption of the Hunga Tonga Hunga Ha'apai volcano". They explained that this corresponds to "a caldera collapse event in which the collapse of this material causes a disturbance in the water column located immediately above the crater". Figure 2 shows the location of the tide gauges on the coast of Peru at the following points: 1) Callao (Figure 2a) and on the coast of Chile (Figure 2b) at points: 1) Arica; 2) Iquique; 3) Mejillones; 4) Antofagasta; 5) Chañaral; 6) Caldera; and 7) Coquimbo. Figure 3 shows some tide gauge records on January 15, 2022, from the tide gauges at stations in Callao, Peru (Figure 2a) [10]. Figures 4 and 5 show records at the following stations on the coast of Chile (Figure 3b): 1) Arica; 4) Antofagasta; 5) Chañaral; 6) Caldera; and 7) Coquimbo. The data from the tide gauges were obtained from Chilean colleagues (Jorge Van Den Bosch Fernandez, Director of the Centro Ingeniería Mitigación Catástropes Naturales Facultad de Ingeniería (CIMCN), University of Antofagasta, Antofagasta, Chile) .

(*a*) (*b*)

Figure 2. (*a*) Location of Callao station, Peru. The tide gauges are marked with a red circle; (*b*) Location of tide gauges on the Chilean coast. The tide gauges are marked with red circles and numbered: 1 – Arica; 2 – Iquique; 3 – Mechellones; 4 – Antofagasta; 5 – Chañaral; 6 – Caldera; 7 – Coquimbo; and 8 – Niuentue. [10,11]

In Figures 3 and 4, the vertical green line indicates the moment of the volcano explosion, the vertical gray line corresponds to the time of arrival of the sea waves to the tide gauge, possibly caused by the Lamb acoustic wave, and the vertical blue line indicates the time of arrival of the tsunami waves to the tide gauge.

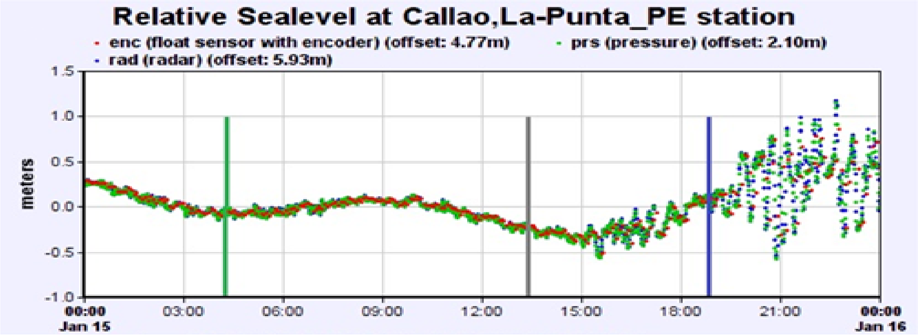

Figure 3. Record from a tide gauge at Callao station, Peru, for January 15, 2022 [12].

According to the tide gauge record in Figure 3, the first waves reached the coast of Callao, Peru, 9 hours after the eruption. It should be noted that the record on these tide gauges begins at 00:00 on January 15, and the explosion occurred at 4:15; if we add 9–10 hours to the time of the explosion, when the early arrival waves began to be observed, we will obtain the interval of 13–14 hours marked on the tide gauge records by a vertical gray line. All records (Figures 3–5) show that stronger waves can be seen on the tide gauges after the arrival of the first weak waves, which coincides with the estimated arrival time of long sea waves (tsunamis); this may indicate that tsunami waves were formed at the moment of the explosion. On the following tide gauge records (Figure 5), which were obtained from the Department of Physics of the University of Santiago, Chile, the time count begins precisely from the moment of the eruption of the Tonga volcano, that is, the first waves arrived on the coast of Chile 9 hours after the eruption of the volcano. Table 2 shows the results of the assessment of the approach time to the tide gauges on the coast of Chile for both tsunami waves and waves caused by the Lamb acoustic wave after the eruption of the Hunga Tonga volcano [8,9]. However, it should be noted that the work considers a possible pre-eruption landslide process as a result of the preparation of the volcanic eruption, and not after it. Since the time of the pre-eruption landslide is unknown, several indirect data suggest that it occurred 4–5 hours before the eruption of the volcano. According to the available literature data on the timing of seismic activity, two peaks of activity were noted on January 14, 2022 with a magnitude of M = 4.9: 21.16 (100 km near the deep-sea trench) and 23.43 (400 km near the Fiji Islands), well before the eruption of Tonga volcano at 4.15 on January 15, 2022. (see, e.g. [3–7]). Additionally, direct observations of the ocean bottom pressure recorded at DART stations near New Zealand [8] (in NZG, NZH and NZI) support the above possibility in principle.

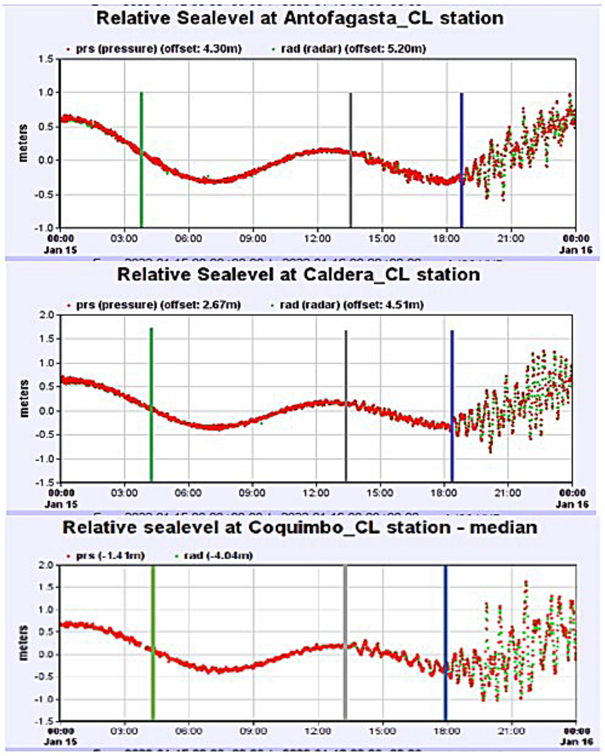

Figure 4. Records from the tide gauges along the coast of Chile for January 15, 2022, obtained from CIMCN (University of Antofagasta, Chile) (the recording on these tide gauges starts from 00:00 on January 15) [11,12].

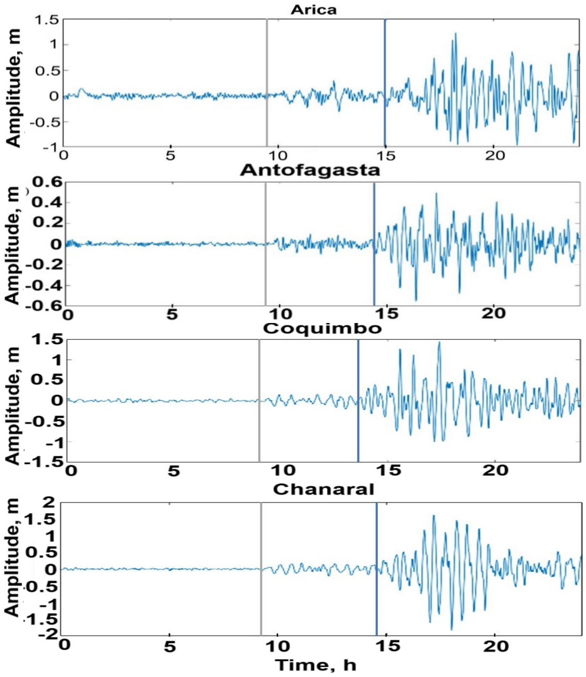

Figure 5. Records from the tide gauges along the coast of Chile for January 15, 2022, obtained from the Department of Physics, University of Santiago, Chile [11–13] (the countdown begins from the moment of the eruption of the Tongo volcano).

Table 2. Results of computing the arrival time of tsunami waves and waves possibly caused by the Lamb acoustic wave after the eruption of the Hunga – Tonga volcano [8,9].

Tide gauge	Distance of tide gauge to volcano, km	Average depth along the path, m	Average long wave velocity along path km/h	Arrival time for tsunami wave h: min	Arrival time for sea waves Lamb waves h:min
Antofagasta	10522	4175	729	14:27	9:33
Arica	10770	4093	721	14:56	9:32
Chanaral	10375	4218	732	14:10	9:11
Cocuimbo	10145	4316	741	13:42	8:58
Caldera	10324	4232	734	14:05	9:08
Mejillones	10544	4143	726	14:32	9:20
Iquique	10707	4123	724	14:47	9:28
Callao	10373	4184	729	14:13	9:11

3. Possible landslide tsunami mechanism during volcanic eruption preparation

The generation of tsunami waves by an underwater landslide formed as a result of preparing a volcanic eruption is one of the most realistic reasons for the appearance of records from the tide gauges before the instruments record the arrival of a normal tsunami wave after a volcanic eruption. To test the hypothesis about the landslide nature of the 'early' tsunami, we will estimate the possibility of an underwater landslide occurring during the preparation of the eruption. The volcano is located near the deep-sea Tonga-Kermadec Basin (Figure 6), which has a fairly steep slope. The basin was formed as a result of the subduction of the Pacific tectonic plate to the west under the Australian plate [3].

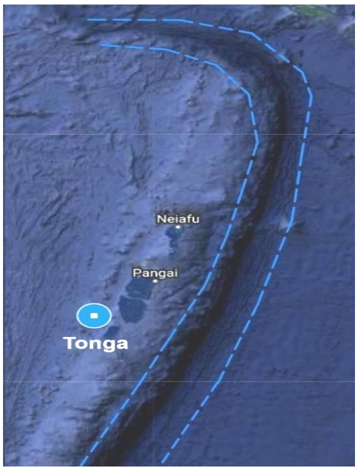

Figure 6. Deep sea Tonga-Kermadec Trench. The trench is marked with a dashed curve. The volcano Tonga is marked by blue dot.

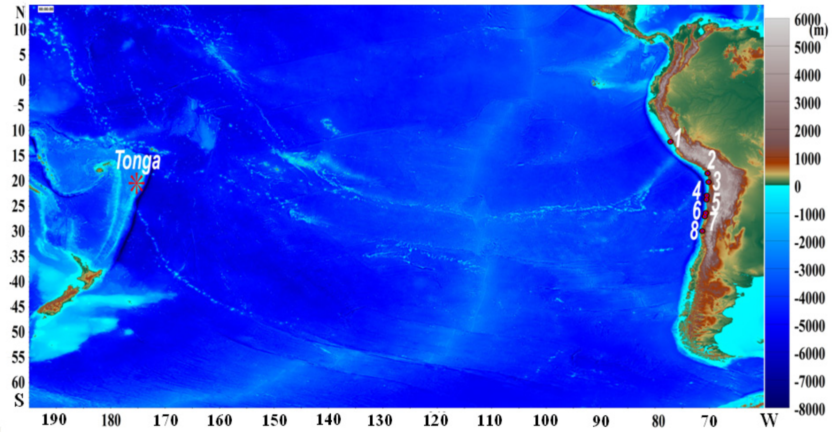

Figure 7. Computation water area. The red asterisk marks the location of the Hunga – Tonga volcano. Numbers 1–8 mark the locations of tide gauges (red circles) along the Chilean coast.

The generation of tsunami waves during the movement of a landslide from the slope of the Tonga volcano and the propagation of the tsunami wave across the Pacific Ocean to the 10-meter isobath were considered [15]. Figure 7 shows the computation water area with the localization of the Hunga Tonga volcano and the tide gauges 1–8 on the coast of Peru and Chile, the data from which are used in the further study. The bathymetry of the Pacific Ocean was used for the modeling, with a spatial step of about 900 m (30″). Modeling was carried out with a time step of 1 s. The considered water area ranged from 190° to 64° W alongside a latitude from 10° N to 65° S. The number of nodes in the numerical scheme is 16,200 × 6400 = 103,680,000 [15,16]. To assess the possible localization of the landslide on the slope, one-dimensional cross-sections of the volcano were made (Figure 8) and the dimensions of the possible landslide were estimated (see Figure 9).

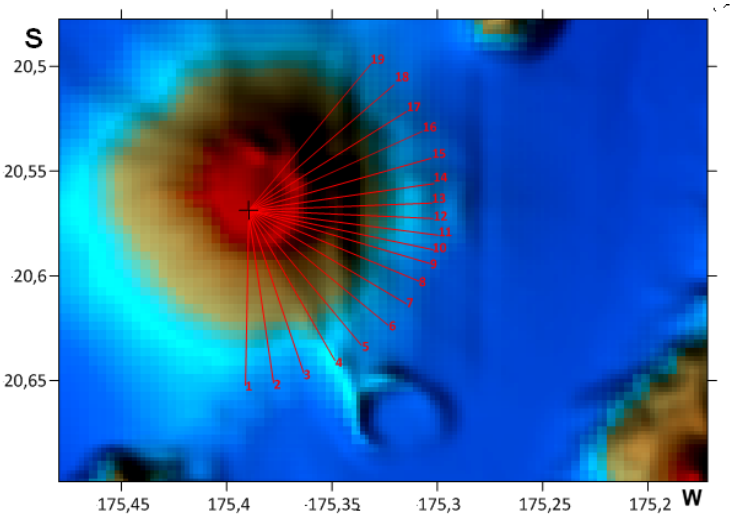

Figure 8. Bathymetry of the Hunga – Tonga volcano in July 2021. Red numbered lines indicate transverse cross-sections.

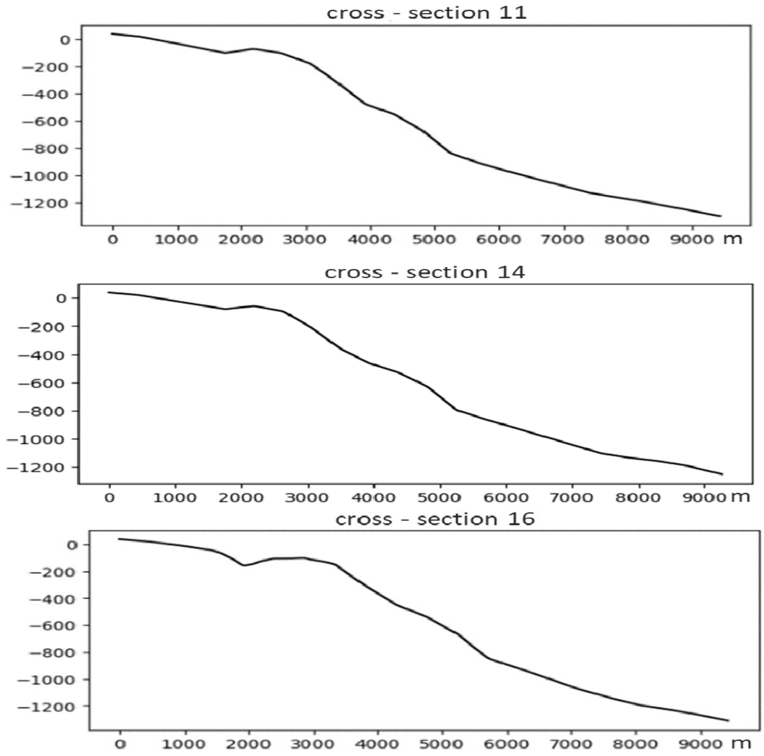

Figure 9. Examples of the bottom relief scheme of the Hunga –Tonga volcano (cross-sections 11, 14, 16) towards the western coast of Chile, which contain possible landslide deposits.

4. Statement of the problem

Landslide bodies in most cases are formed on the underwater slopes, which usually have a high gradient. Volcanic or seismic activity can also lead to the sliding of part of the slope, which can be the source of the formation of a long surface water wave (tsunami). Most tsunami models generated by landslides are based on the response of the sea surface to the movement of the solid bottom. There are several models that describe the movement of landslide masses (e.g., a rigid body model, a visco-plastic fluid model, and an elastic-plastic fluid model). Using available information on existing types of landslides (see, e.g., [17–21]), we combined the landslide process as a rigid body, which consisted of many segmental blocks, and the landslide process was modeled by the dynamic vertical displacement of segmental blocks along the landslide slope, thus imitating the sliding of the landslide mass [22–24]. The kinematics of the block movement is determined by the schematic behavior of the landslide movement, which corresponds to a typical implementation of the computation within the elastoplastic model: sliding of the upper part of the landslide layer with a simultaneous increase in the thickness of the lower part of the slope (Figures 10–12) (for more details, see, e.g., [23,24]). Modeling of the landslide process was carried out for three scenarios within the framework of a rigid segmental model (Scenario 1,2). For all 3 Scenarios, the thickness of the sedimentary layer is about 50 m. Figure 10 shows a schematic representation of the movement of a landslide body along an underwater slope, which consists of 7 segments (Scenario 1). For this Scenario (Figure 10), a landslide with a length of 4.6 km and a width of 0.8 km is considered. The sliding of the landslide mass can be approximated quite roughly by the displacement of the upper segmental blocks downward, with the simultaneous displacement of the corresponding virtual segmental blocks 8–14 upward (Figure 10a). Each reverse movement takes 20 sec. The final position of the landslide body is shown in Figure 10b.

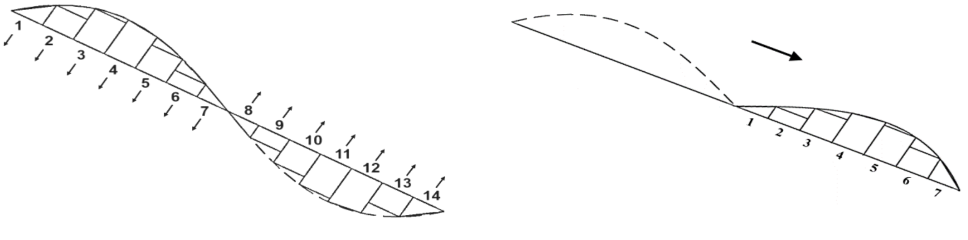

(*a*) (*b*)

Figure 10. Schematic representation of the displacement of the landslide body along the underwater slope for Scenario 1.

For Scenario 2 (Figure 11), a large landslide is considered. The number of segmental blocks was also 7. The blocks moved sequentially one after another. For Scenario 2, in contrast to Scenario 1, the movement of the segmental blocks occurs in 4 stages. The movement times of the segments are different.

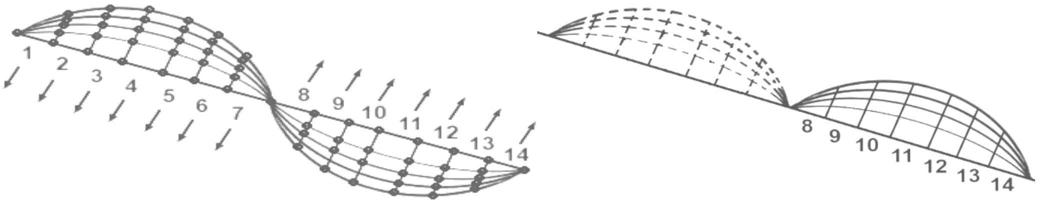

(*a*) (*b*)

Figure 11. Schematic representation of the displacement of a landslide body along an underwater slope for Scenario 2.

Analogous to Scenario 1, the movement of segments 1–7 was accompanied by the simultaneous symmetrical movement of the virtual segmental blocks 8–14 (Figure 11a,b), and the movement of a landslide down the slope is simulated. The final position of the landslide body is shown in Figure 11b.

For Scenario 3, the process of displacement of the landslide mass along the slope also occurs in 4 stages, each of which takes a different time. As can be seen from the schematic representations in Figures 11 and 12, each decrease in the thickness of the landslide corresponds to a simultaneous increase in the thickness of the lower part of the slope.

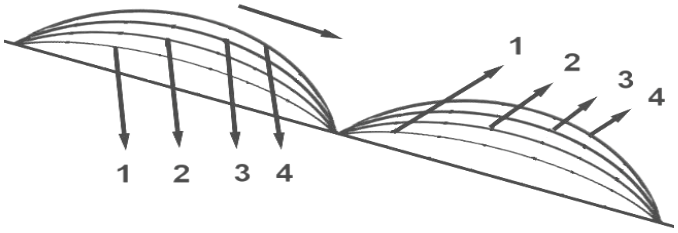

Figure 12. Schematic representation of the displacement of a landslide body along an underwater slope for Scenario 3.

In all three Scenarios, it was assumed that the process ends when the velocity of the leading edge of the landslide masses becomes zero. It is well known that a landslide begins to move at a certain critical value of the stress in which it arises. The critical stress starts when the landslide begins to move; for this process, this could be both minor seismic foreshocks, of which there were many before the eruption, and the process of preparing the eruption itself, during which a process of stress accumulation occurs, thereby gradually increasing to the limit, at which and the volcano erupted. In this regard, the moment of realization of the critical stress can only be determined by solving the inverse problem based on the moment of arrival of the first wave train to a concrete coast.

5. Numerical simulation of the process of sliding on the slope of a volcano

5.1. Mathematical formulation of the problem

This work solves the problem of an underwater landslide generating a wave on the water surface. To describe the generation and propagation of a wave by an underwater landslide (Figures 10–12), shallow water equations were used in the following form [22–25], where x, y are the spatial coordinates along the Ox and Oy axes, respectively, t is the time, $u(x, y, t)$ and $v(x, y, t)$ are velocity components along the Ox and Oy axes, respectively, g is the gravity acceleration, h is the maximum depth of the basin, and $\eta(x, y, t)$ is the perturbation of the free surface relative to its undisturbed level (Figure 13).

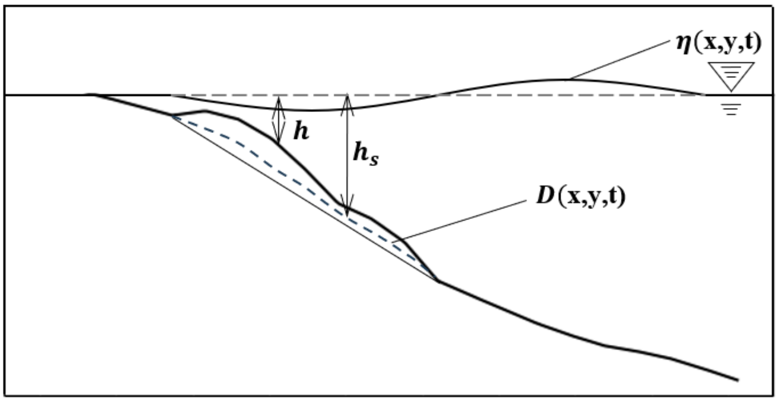

Figure 13. Schematic representation of the generation of a long wave on the surface of water.

$$\frac{\partial u}{\partial t}+u\frac{\partial u}{\partial x}+v\frac{\partial u}{\partial y}+g\frac{\partial \eta}{\partial x}=fu-\frac{r}{h}u\sqrt{u^2+v^2}\ , \tag{1}$$

$$\frac{\partial v}{\partial t}+u\frac{\partial v}{\partial x}+v\frac{\partial v}{\partial y}+g\frac{\partial \eta}{\partial y}=-fv-\frac{r}{h}u\sqrt{u^2+v^2}\ , \tag{2}$$

$$\frac{\partial \eta}{\partial t}=\frac{\partial D}{\partial t}-\frac{\partial h_s}{\partial t}-\frac{\partial}{\partial x}\big((h_s+\eta-D)u\big)-\frac{\partial}{\partial y}\big((h_s+\eta-D)v\big). \tag{3}$$

The value $D(x, y, t)$ determines the change in the thickness of the landslide during the sliding process (Figure 13), $H(x, y, t) = h(x, y, t) + \eta(x, y, t)$ – total depth, r is the coefficient of bottom friction ($r = 0.04$), $f = 2\Omega\cos\theta$ is the Coriolis parameter, Ω is the Earth angular speed, θ is the latitude, and $h(x, y, t) = h_s(x, y, t) - D(x, y, t)$.

The initial conditions have the following form:

$$\eta(x,y,0)=0,\ \ u(x,y,0)=0,\ v(x,y,0)=0. \tag{4}$$

The normal velocity component at the free boundary is found as $u_n=\dfrac{c\eta}{H+\eta}$ ($c=\sqrt{gH}$), and the boundary conditions of the “solid wall” are selected in the form $u_n = 0$. To solve equations (1)–(3), the difference scheme of A. Sileski was used [26].

5.2. Generation of a tsunami source by a landslide source

The water area includes part of the coast of Chile and Peru, since most of the records from the tide gauges (obtained from colleagues in Chile) (Figures 5, 7 and 8) are located on these coasts. The paper considers three scenarios for modeling the movement of a pre-eruption landslide source along the slope of a volcano and the corresponding formation of a tsunami source with different dynamic characteristics of the landslide body.

Scenario 1

For Scenario 1, a landslide on the slope of a volcano with a location in Figure 10 was considered. The number of segmental blocks that make up the landslide was 7. The blocks moved sequentially one after another, every 10 seconds. The displacement times varied depending on the blocks (i.e., 1–10 sec, 2–20 sec, 3–30 sec, 4–40 sec, 5–10 sec, 6–20 sec, 7–30 sec). Simultaneously, with the displacement of segments 1–7, segments 8–14 shifted upward symmetrically (Figure 10), thus imitating the movement of a landslide down the slope. The maximum wave displacement in the landslide source for this scenario reached 35 m. Figure 14 shows 6 time moments of the tsunami source formation under implementation of Scenario 1. It is clearly seen that the wave front has an almost rounded shape at the time moment t = 20 sec; however, starting from t = 30 sec, the tsunami wave front extends in the direction of the landslide.

To evaluate the modeling results, the computed tide gauge records were compared with the field data. Figures 15–16 show a comparison of the field and computation data for Scenario 1 for the points of Antofagasta, Chañaral, Coquimbo, and Arica since wave displacements are most characteristic in the field records obtained from these points. It is clearly seen that the wave front has an almost rounded shape at the time *t* = 20 sec; however, starting from *t* = 30 sec, the tsunami wave front is elongated in the direction of the landslide.

In Figure 15, the histogram of the wave heights along the coast of Chile and Peru obtained under simulation of Scenario 1 is presented. The maximum wave heights were registered at the part of Chilean coast between 24° and 25° S and reach 0.8 m.

For a more detailed analysis of the wave approach, Figure 16 shows the recordings from the virtual tide gauges during the simulation of Scenario 1. To evaluate the results of the simulation, the computed tide gauge records from Scenario 1 were compared with the field data for the points Antofagasta, Chanyaral, Cocimbo, and Arica since the field records obtained for these points wave displacements are most characteristic.

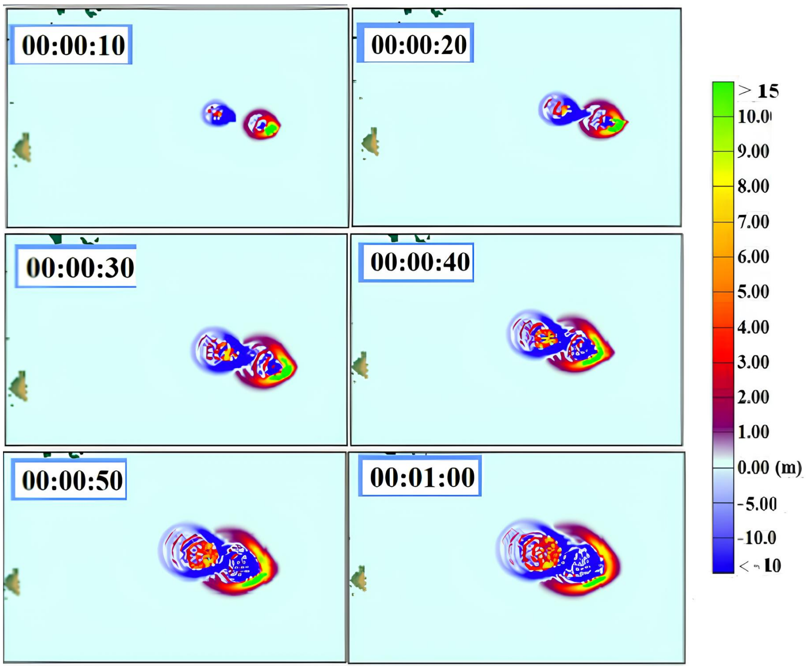

Figure 14. Formation of a tsunami source for 6 time moments during the movement of a landslide along the slope of a volcano.

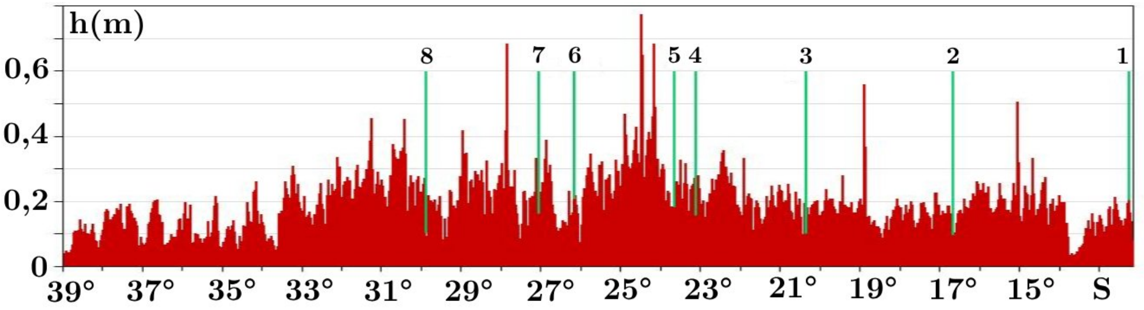

Figure 15. Histogram of the distribution of maximum wave heights along the coast of Chile and Peru during the simulation of Scenario 1. The tide gauges are marked with green lines and numbered as follows: 1 – Callao; 2 – Arica; 3 – Iquique; 4 – Mejillones; 5 – Antofagasta; 6 – Chañaral; 7 – Caldera; and 8 – Coquimbo.

Since we have no information about the time of the landslide, we can assume that it occurred 4–5 hours before the volcano erupted. According to the records in Figure 3, the first waves reached the coasts of Peru and Chile about 9 hours after the eruption, while the main tsunami wave generated by the volcanic eruption arrived 14–15 hours later (see Table 2). This is the interval that we analyze in our scenarios. For scenario 1, the wave behaviors of both the full-scale and the calculated tide gauge records are quite close (Table 3). However, some maximum peaks are 1.5 times higher than the calculated values. Therefore, Scenario 2 with the landslide shown in Figure 11 was considered for a further analysis.

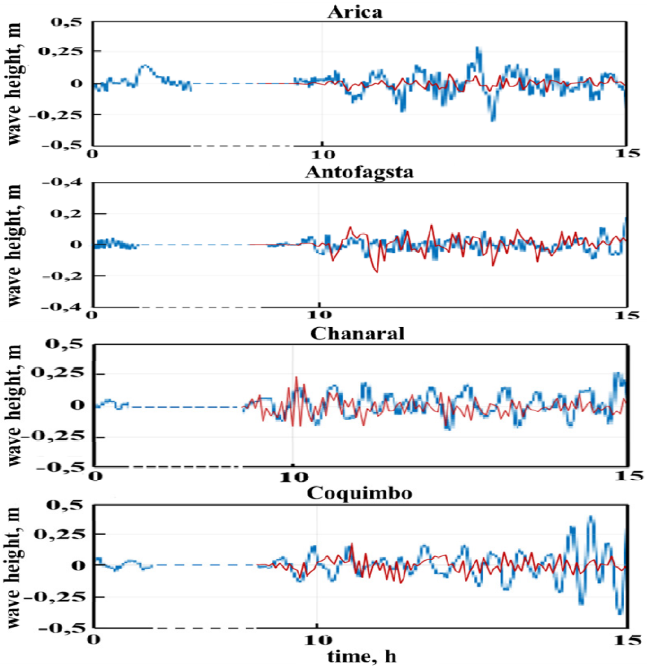

Figure 16. Comparison of records from real and virtual tide gauges for the Arica, Antofagasta, Chañaral, and Coquimbo. The red line is the results of the numerical simulation, the blue line is a real record. The dashed line indicates a break in the recording.

Table 3. Comparison of computation results for Scenario 1 with field data.

Tide gauge	Callao (−12.07, −77.16)	Arica (−18.47, −70.32)	Iquique (−20.20, −70.14)	Mejillones (23.09, -70.45)	Antofagasta (−23.65, −70.40)	Chanaral (−26.35, −70.63)	Caldera (−27.06, −70.82)	Coquimbo (−29.94, −71.33)
Real data, m	0.19	0.3	0.10	0.21	0.10	0.20	0.09	0.17
Scenario 1, max, m	0.15	0.09	0.13	0.17	0.16	0.19	0.23	0.14

Scenario 2

For scenario 2 (Figure 11), a landslide with a landslide body length on the volcano slope of about 6 km, a landslide width of about 1 km, and a sedimentary layer thickness of about 0.05 km were considered, while the number of segmental blocks into which the landslide is divided is also 7. The blocks moved sequentially one after another (see Table 4). For scenario 2, in contrast to scenario 1, the movement of the segmental blocks occurs in 4 stages. From Table 4, that the movement of segments 1–7 was accompanied by the simultaneous symmetrical movement of the virtual segmental blocks 8–14 (see Figure 11a).

Table 4. Movement of segmental blocks according to Scenario 2.

Step	Block number	1	2	3	4	5	6	7	8	9	10	11	12	13	14
First step	Start time of movement (s)	0	0	0	0	0	0	0	0	0	0	0	0	0	0
	Time of movement (s)	10	5	10	15	10	15	5	10	15	5	15	10	15	5
	Block offset (m)	−2	−4	−8	−10	−8	−4	−2	2	4	8	10	8	4	2
Second step	Start time of movement (s)	10	5	10	15	10	15	5	10	15	5	15	10	15	5
	Time of movement (s)	5	10	15	10	20	10	10	5	10	15	20	15	10	15
	Blocks offset (m)	−4	−6	−10	−15	−10	−6	−4	4	6	10	15	10	6	4
Third step	Start time of movement (s)	15	15	25	25	30	25	20	15	25	20	30	25	25	20
	Time of movement (s)	10	15	20	25	5	10	20	10	15	20	25	5	10	20
	Blocks offset (m)	−4	−6	−10	−15	−10	−6	−4	4	6	10	15	10	6	4
Fourth step	Start time of movement (s)	25	30	40	40	40	40	40	40	40	40	40	40	40	40
	Time of movement (s)	25	30	35	10	15	20	25	10	20	10	10	20	20	20
	Blocks offset (m)	−2	−4	−8	−10	−8	−4	−2	2	4	8	10	8	4	2
Final time of movement (s)		50	60	80	60	50	55	60	35	50	60	70	50	55	60

Figure 17 shows the origin of a tsunami source during the movement of a landslide body along the slope of a volcano and the further propagation of a tsunami wave within the water area under consideration for 6 time moments.

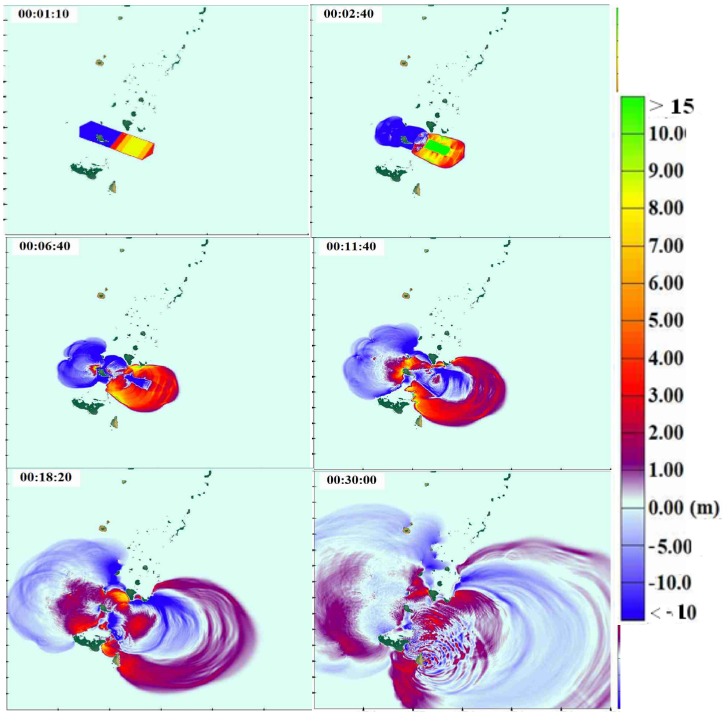

Figure 17. Generation of a tsunami source and propagation of waves over part of the computation water area.

Figure 18 shows the computed records of the tide gauges for 6 points along the coast of Chile for scenario 2. In Figure 18, the blue line indicates the time of arrival of the early tsunami waves caused by the landslide. Since we have no information about the time of the landslide process, we can assume that it began 4–5 hours before the volcanic explosion (gray line), which is the interval that we analyze. In the analyzed intervals (from the gray to the blue line), the wave height on the 10-meter isobath did not exceed 50 cm. Figure 19 shows the two-dimensional distribution of the maximum wave heights on the 10-meter isobath for the Peru-Chile coastline for scenario 2. For the given dynamics of the landslide body movement, the obtained results correlated better with the field data (Table 5). However, to further clarify the possible landslide process during the preparation of a volcanic eruption, scenario 3 was considered, the model of which is distinguished by the dynamics of the movement of the segmental blocks close to the implementation of the calculation within the framework of the elastic-plastic model: a landslide of the upper part of the landslide layer with a simultaneous increase in the thickness of the lower side of the slope (see Figure 12).

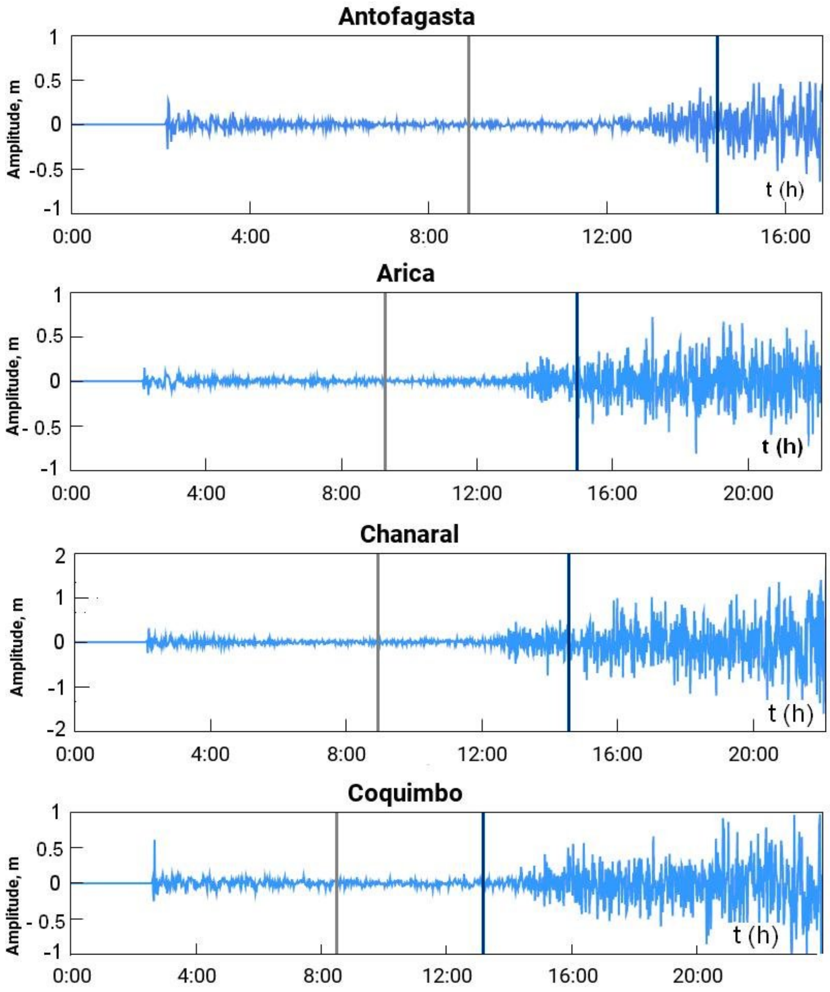

Figure 18. Computed tide-gauge records for 6 points on the Chilean coast for Scenario 2.

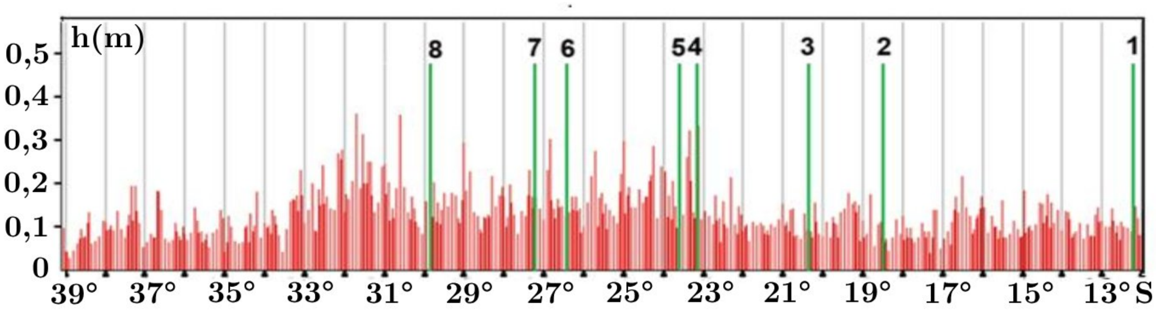

Figure 19. Histogram of the of maximum wave height distribution along the coast of Chile and Peru during the simulation of Scenario 2. Points are marked with green lines and numbered as follows: 1 – Callao; 2 – Arica; 3 – Iquique; 4 – Mejillones; 5 – Antofagasta; 6 – Chañaral; 7 – Caldera; and 8 – Coquimbo.

Table 5. Comparison of computed results for Scenario 1 with field data.

	Earthquake data							
No.	1	2	3	4	5	6	7	8
Points Data	Callao	Arica	Iquique	Mejillones	Antofagasta	Chanaral	Caldera	Coquimbo
Real data, m	0.19	0.3	0.10	0.21	0.10	0.20	0.09	0.17
Scenario 2, max, m	0.15	0.09	0.12	0.18	0.15	0.17	0.21	0.12

Scenario 3

The difference between scenario 3 and scenarios 1 and 2 is that the process of moving the landslide masses along the slope occurs in 4 stages; at each stage, the displacement of the segments occurs simultaneously, and each stage takes a finite time: 10 s, 20 s, and 10 s and 20 s (see Table 6).

Table 6. Movement of segmental blocks according to Scenario 3.

Step	Block number	1	2	3	4	5	6	7	8	9	10	11	12	13	14
First step	Start time of movement (s)	0	0	0	0	0	0	0	0	0	0	0	0	0	0
	Time of movement (s)	10	10	10	10	10	10	10	10	10	10	10	10	10	10
	Block offset (m)	−2	−4	−8	−10	−8	−4	−2	2	4	8	10	8	4	2
Second step	Start time of movement (s)	10	10	10	10	10	10	10	10	10	10	10	10	10	10
	Time of movement (s)	20	20	20	20	20	20	20	20	20	20	20	20	20	20
	Blocks offset (m)	−4	−6	−10	−15	−10	−6	−4	4	6	10	15	10	6	4
Third step	Start time of movement (s)	30	30	30	30	30	30	30	30	30	30	30	30	30	30
	Time of movement (s)	10	10	10	10	10	10	10	10	10	10	10	10	10	10
	Blocks offset (m)	−4	−6	−10	−15	−10	−6	−4	4	6	10	15	10	6	4
Fourth step	Start time of movement (s)	40	40	40	40	40	40	40	40	40	40	40	40	40	40
	Time of movement (s)	20	20	20	20	20	20	20	20	20	20	20	20	20	20
	Blocks offset (m)	−2	−4	−8	−10	−8	−4	−2	2	4	8	10	8	4	2
Final time of movement (s)		60	60	80	60	60	60	60	60	60	60	60	60	60	60

The generation of a tsunami source with such a landslide displacement along the slope is shown in Figure 20. The entire process of sliding, and thus the formation of a tsunami source, takes 60 s. Figure 21 shows one of the moments in the time of tsunami wave propagation in the computed water area.

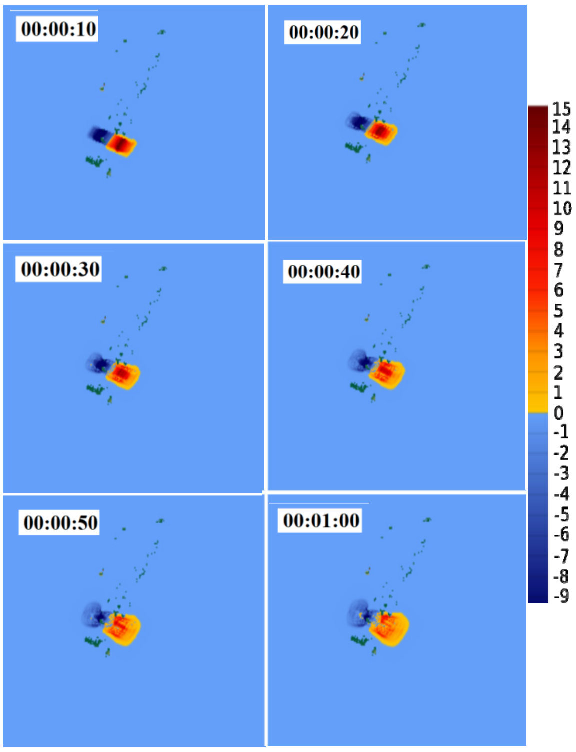

Figure 20. Formation of a tsunami source for 6 time moments when a landslide moves along the slope of the volcano.

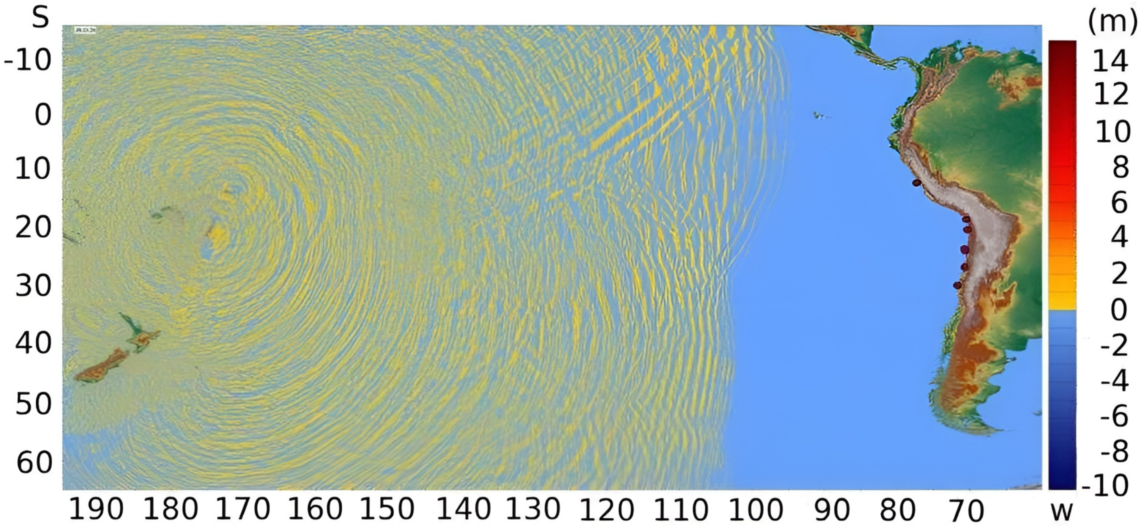

Figure 21. Propagation of a tsunami wave over the computation water area 7 hours 26 min after the end of the sliding process.

Figure 22 shows the 2D distribution of the maximum wave heights on a 10-meter isobath for the section of the coast of Peru-Chili during the implementation of Scenario 3.

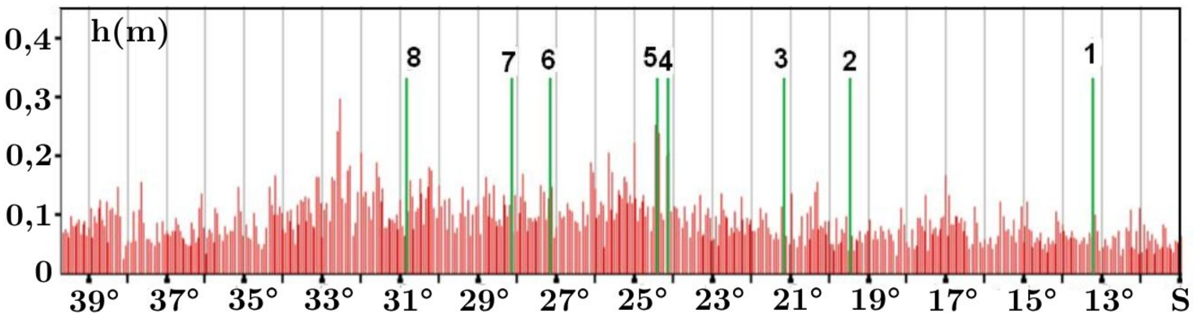

Figure 22. 2D distribution of maximum wave heights along the coast of Peru-Chile. The points are marked with green lines and numbered as follows: 1 – Callao; 2 – Arica; 3 – Iquique; 4 – Mejillones; 5 – Antofagasta; 6 – Chañaral; 7 – Caldera; and 8 – Coquimbo.

In Table 7, the values of the maximum wave heights for 8 coastal points are presented.

Table 7. Comparison of computed results for Scenario 1 with field data.

	Earthquake data							
No.	1	2	3	4	5	6	7	8
Points Data	Callao	Arica	Iquique	Mejillones	Antofagasta	Chanaral	Caldera	Coquimbo
Real data, m	0.19	0.3	0.10	0.21	0.10	0.20	0.09	0.17
Scenario 3, max, m	0.14	0.11	0.09	0.12	0.11	0.15	0.15	0.14

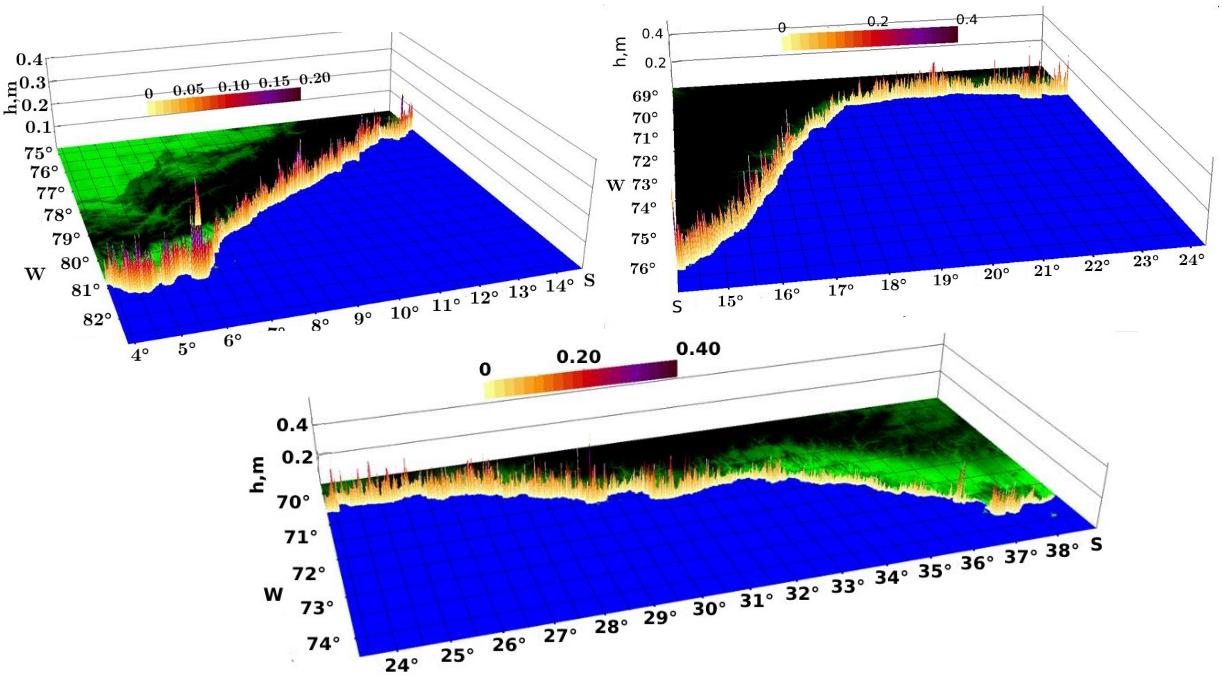

Figure 23. 3D histograms of the distribution of maximum wave heights on a 10-m isobath.

Figure 23 shows the 3D distribution of the maximum wave heights for different parts of the coast on a 10-m isobath for the section of the coast of Peru-Chili during the implementation of Scenario 3.

5. Conclusions

This paper proposed a mechanism for the formation of "early" tsunami waves on the Pacific coast that occurred after the eruption of the Tunga volcano 4–5 hours earlier than the possible time of the wave arrival at a concrete tide gauge. The paper shows that in addition to the hypotheses available in the literature that explain this phenomenon as the generation of tsunami waves by Lamb waves or the collapse of the Calders, another hypothesis is possible regarding the generation of early waves by a pre-eruption landslide localized on the slope of the Tonga volcano. At the same time, during the preparation period for the eruption, as the maximum stress accumulated, the trigger mechanism for the landslide movement could have been both numerous small seismic shocks and the preparation process for the volcanic eruption itself. The characteristics of the tsunami generated by the pre-eruption landslide process on the slope of the volcano were obtained. Considering various scenarios of the pre-eruption landslide source formation and taking the tsunami characteristics data in specific tide gauges into account, it was found that the heights of early waves suitable for the Peru-Chile coast are quite close to the values recorded by real tide gauges at eight points under consideration, regardless of the nature of the pre-eruption landslide process dynamics (Table 8).

Table 8. Comparison of natural data with computed data for three Scenarios.

Points	Real data, m	Scenario 1, max, m	Scenario 2, max, m	Scenario 3, max, m
Callao	0.19	0.15	0.15	0.14
Arica	0.3	0.09	0.09	0.11
Iquique	0.10	0.13	0.12	0.09
Mejillones	0.21	0.17	0.18	0.12
Antofagasta	0.1	0.16	0.15	0.11
Chanaral	0.2	0.19	0.17	0.15
Caldera	0.09	0.23	0.21	0.15
Coquimbo	0.17	0.14	0.12	0.14

Author contributions

Conceptualization, R.K.M., J.V.D.B.F. and A.K.; methodology, R.M., J.V.D.B.F. and A.K.; software, I.S.,D.S,K.P; validation, R.K.M., J.V.D.B.F. formal analysis, R.K.M., J.V.D.B.F; investigation, R.K.M. and A.K.; resources, J.V.D.B.F. and A.K, data curation, R.K.M. and J.V.D.B.F.; writing—original draft preparation, I.S., K.P; writing—review and editing, R.K.M., A.K. and J.V.D.B.F.; visualization, I.S.,D.S, K.P. and R.K.M.; supervision, R.K.M. and A.K.; project administration, R.K.M.; funding acquisition, A.K. and J.V.D.B.F.; All authors have read and agreed to the published version of the manuscrip

Use of Generative-AI tools declaration

The authors declare they have not used Artificial Intelligence (AI) tools in the creation of this article.

Acknowledgments

The work was supported by the Laboratory of Nonlinear Hydrophysics and Natural Disasters of the Ilychev Pacific Oceanological Institute, a grant from the Ministry of Science and Higher Education of the Russian Federation (agreement No. 075-15-2022-1127 dated 01.07.2022).

Conflict of interest

All authors declare no conflicts of interest in this paper.

References

1. Nosov MA, Bolshakova AV, Sementsov KA (2021) Energy characteristics of tsunami sources and the mechanism of wave generation by seismic movements of the ocean floor. *Moscow Univ Phys* 76: S136–S142. https://doi.org/10.3103/S0027134922010076
2. Paris R (2015) Source mechanisms of volcanic tsunamis. *Philos Trans R Soc A* 373: 20140380. https://doi.org/10.1098/rsta.2014.0380
3. Terry JP, Goff J, Winspear N, et al. (2022) Tonga Volcanic Eruption and Tsunami, January 2022: Globally the Most Significant Opportunity to Observe an Explosive and Tsunamigenic Eruption Since Ad 1883 Krakatau. *Geosci Lett* 9: 24. https://doi.org/10.1186/s40562-022-00232-z
4. Moodie K (2022) Tonga eruption likely the world's largest in 30 years—scientist. Available from: https://www.rnz.co.nz/news/world/459657/tonga-eruption-likely-the-world-s-largest-in-30-years-scientist. (visited on 02/09/2024)
5. Headarzadeh M, Gusman AR, Ishibe T, et al. (2022) Estimating the eruption-induced water displacement source of the 15 January 2022 Tonga volcanic tsunami from tsunami spectra and numerical modelling, *Ocean Eng* 261: 112165. https://doi.org/10.1016/j.oceaneng.2022.112165.
6. Fujii Y, Satake K (2024) Modeling the 2022 Tonga Eruption Tsunami Recorded on Ocean Bottom Pressure and Tide Gauges Around the Pacific. *Pure Appl Geophys* 181: 1793–1809. https://doi.org/10.1007/s00024-024-03477-1
7. Lynett P, Mccann M, Zhou Z, et al. (2022) Diverse tsunamigenesis triggered by the Hunga Tonga-Hunga Ha'apai erupation. *Nature* 609: 728–733. https://doi.org/10.1038/s41586-022-05170-6
8. Omira R, Ramalho RS, Kim J, et al. (2022) Global Tonga tsunami explained by a fast-moving atmosphereic source. *Nature* 609: 734–740. https://doi.org/10.1038/s41586-022-04926-4

9. Ren Z, Higuera P, Li-Fan Liu P (2023) On Tsunami Waves Induced by Atmospheric Pressure Shock Waves After the 2022 Hunga Tonga-Hunga Ha'apai Volcano Eruption. *J Geophys Res-Oceans* 128: e2022JC019166. https://doi.org/10.1029/2022JC019166
10. Wikipedia (2022) Hunga Tonga–Hunga Ha'apai eruption and tsunami. Available from: https://en.wikipedia.org/wiki/2022_Hunga_Tonga–unga_Ha'apai_eruption_and_tsunami#:~:text=In%20December%202021%2C%20an%20eruption,main%20island%2C%20and%20is%20part. (visited on 02/05/2024)
11. Gebco Digital Atlas electronic bathymetry [Electronic resource]. Available from: https://www.gebco.net/data_and_products/gridded_bathymetry_data/gebco_2024/.
12. Sea Level Station (2022) "Sea Level Monitoring Stations, Caldera, Coquimbo, Antofagasta, Mejillones, Iquiqu Ary 2022" UNESCO. Available from: https://www.ioc-selevelmonitoring.org/.
13. Rara, destructiva y difícil de modelar: las características únicas de la erupción volcánica ocurrida en Tonga, 2022. Available from: https://uchile.cl/noticias/183755/las-caracteristicas-unicas-de-la-erupcion-volcanica-ocurrida-en-tonga. (visited on 01/26/2024)\
14. Mauricio F (2022) "Las características únicas de la erupción volcánica ocurrida en Tonga" Programa Académico de Bachillerato; Programa de Riesgo Sísmico. U. de Chile. Chile.
15. Lobkovsky LI, Mazova RKh, Baranova NA, et al. (2022) Possible Seismic Source Mechanism of the Catastrophic Tsunamigenic Earthquake on May 9, 1877 in Northwestern Chile. *Pure Appl Geophys* 180: 1695–1715. https://doi.org/10.1007/s00024-022-03149-y
16. Mazova RKh, Kurkin AA, Okunev DA (2022) Numerical modeling of a tsunami of landslide origin in the Kuril Basin. *Sci Tsunami Hazards* 41: 352–369.
17. Iwasaki SI (1989) Tsunami generated by a horizontal motion of a landslide in a ocean, *Abstracts of papers of International tsunami meetings, July 31–August 10, Novosibirsk, Russia*, 2.
18. Fine IV, Kulikov EA, Rabinovich AB (2000) Thunami generation by subaerial landslides, *Abstracts of The International Workshop "Tsunami Risk Assessment Beyond 2000", 14–16 June 2000, Moscow, Russia*, 53.
19. Harbitz CB (1999) On tsunami characteristics and submarine slide dynamics, *Proc. International Conference on Tsunamis, 26–28 May 1998, Paris, France*, 258–264.
20. Watts P, Imamura F, Grilli S (2000) Comparing model simulations of three benchmark tsunami generation cases. *Sci Tsunami Hazards* 18: 115–123.
21. Jiang L, LeBlond PH (1993) Numerical modelling of an underwater Bingham plastic mudslide and the waves which it generates. *J. Geophys Res* 98: 10303–10317. https://doi.org/10.1029/93JC00393
22. Garagash IA, Lobkovsky LI, Kozyrev OR, et al. (2003) Generation and runup of tsunami waves at an submarine landslide. *Oceanology* 43: 173–181.
23. Papadopoulos GA, Lobkovsky LI, Mazova RKh, et al. (2007) Numerical Modeling of Sediment Mass Sliding and Tsunami Generation: the Case of 7 February 1963, in Corinth Gulf, Greece. *Mar Geod* 30: 335–344. https://doi.org/10.1080/01490410701568541
24. Mazova R.Kh, Suchkov AA, Kurkin AA (2023) Assesment of the maximum tsunami wave heights on the Crimea-Caucasus coast of the Black sea from possible underwater earthquakes and landslidesin the Dzhubga area. *Sci Tsunami Hazards* 42: 146–158.

25. Voltzinger NE, Klevanny KA, Pelinovsky EN (1989) Long-wave dynamics of the coastal zone, *Hydrometeoizdat: Leningrad*, 272. Available from: http://elib.rshu.ru/files_books/pdf/img-428155120.pdf
26. Sielecki A, Wurtele M (1970) The numerical integration of the nonlinear shallow-water equations with sloping boundaries. *J Comput Phys* 6: 219–236. https://doi.org/10.1016/0021-9991(70)90022-7